Chapter 15
Application to Mobile Robot RMP

Abstract In this chapter, the application of the ZD approach is further investigated to the velocity-level RMP of mobile redundant robot manipulators. That is, by introducing three different ZFs and by exploiting the ZD design formula, we propose, develop, and investigate a velocity-level RMP performance index. Then, based on such a performance and with physical limits considered, the resultant RMP scheme is presented and investigated to remedy the joint-angle drift phenomenon of mobile redundant robot manipulators. Such a scheme is reformulated as a QP, which is solved by a numerical algorithm. With two path-tracking examples, simulation results based on a wheeled mobile robot manipulator substantiate well the effectiveness and accuracy of the proposed velocity-level RMP scheme (as well as show the application prospect of the presented ZD approach once again).

15.1 Introduction

As presented in Chap. 14, fixed-base redundant robot manipulators (e.g., the PUMA 560 robot manipulator) have long been studied and widely applied in factory automation [1–8]. In addition, many techniques have been developed and investigated for motion planning of fixed-base redundant robot manipulators. The most popular method is to apply the pseudoinverse formulation for obtaining a general solution at the joint-velocity and/or joint-acceleration level, which contains a minimum-norm particular solution and a homogeneous solution [9–12]. However, this method has the generally undesirable property that repetitive end-effector motions do not necessarily yield repetitive joint motions. Thus, the manipulator's behavior is difficult to predict when the end-effector traces a closed path in its workspace. In addition, it is less efficient to readjust the manipulator's configuration after every cycle via self-motion such that the joint angles return to their initial values. In the last three decades, a large number of research on the topic of repetitive motion have been produced [5, 13–18] (see also Chap. 14).

With the evolution of the complex technological society and the introduction of new notions and innovative theoretical tools in the field of intelligent systems, mobile manipulators are attracting significant interest in the industrial, military, and public

Y. Zhang and D. Guo, *Zhang Functions and Various Models*,
DOI 10.1007/978-3-662-47334-4_15

service communities [19–22], because of their large-scale mobility and manipulation abilities, as compared to these of the fixed-base manipulators. In general, a mobile manipulator is a robotic device composed of a mobile platform and a stationary robot manipulator fixed to the platform. However, the integration of a redundant robot manipulator and a mobile platform gives rise to many new difficulties; for example, how to coordinate a given task into fine motions to be carried out by the robot manipulator and the gross motions to be achieved by the mobile platform; and how to define the repeatability of a redundancy-resolution scheme for a mobile robot manipulator. It is well known that, for a stationary robot manipulator, an redundancy-resolution scheme is called repetitive, if it maps closed paths in the task space to closed trajectories in the configuration space (see also Chap. 14). However, for a mobile robot manipulator, if the mobile platform does not return to the initial position, a repetitive redundancy-resolution scheme for a stationary robot manipulator is no longer fit for a mobile robot manipulator. Note that repetitive motion control of mobile robot manipulators starts to play a more and more important role in practical applications, which urgently requires an effective scheme for solving the non-repetitive problem of mobile robot manipulators. In [23], Tchoń was the first to introduce the concept of repeatability of inverse kinematics algorithms for mobile robot manipulators by exploiting the endogenous configuration space approach; and further presented repeatable inverse kinematics algorithms [24–26], which provides an insight into the mechanism of repeatability. However, among these inverse kinematics algorithms for repeatability of mobile robot manipulators, the physical constraints (e.g., joint-angle limits and joint-velocity limits) are usually not taken into account. If these physical limits are not considered, a saturation may occur in some cases. Thus, these schemes may be less effective to control mobile robot manipulators for generating cyclic motion.

In this chapter, based on the presented ZD approach, we propose and investigate a novel redundancy-resolution scheme at the velocity level to achieve the RMP purpose of mobile redundant robot manipulators (with physical constraints considered). Specifically, by introducing three different ZFs and by exploiting the ZD design formula [27], a velocity-level RMP performance index is proposed, developed and investigated. To the best of the authors' knowledge, such a new RMP performance index for mobile redundant robot manipulators has never been investigated before by others. Then, a novel RMP scheme is presented by combining the proposed performance index, physical constraints, and integrated kinematical equations of mobile robot manipulators, and further reformulated as a QP subject to equality and bound constraints. As an illustrative example, a wheeled mobile robot manipulator is studied, which is composed of a mobile platform driven by two independent wheels, and a six-DOF spatial robot manipulator mounted on the platform. Tracking-path tasks based on such a wheeled mobile robot manipulator are performed, which further substantiate the efficacy of the proposed RMP scheme and show once again the application prospect of the presented ZD approach. Besides, it is worth pointing out here that, in our previous book [5], the investigation of velocity-level RMP is presented only for fixed-base redundant robot manipulators. By contrast, in this book (or specifically, in this chapter), we focus on investigating the velocity-level RMP for

mobile redundant robot manipulators. Thus, the velocity-level RMP investigation in this chapter can be viewed as an extension of that in [5] (i.e., from the fixed-base robot to the mobile one).

15.2 RMP Performance Index Derived via Different ZFs

In this section, the presented ZD approach is applied to deriving the velocity-level RMP performance index for mobile redundant robot manipulators.

15.2.1 Kinematics Modeling of Mobile Robot Manipulators

In this subsection, a wheeled mobile redundant robot manipulator [21, 22, 28, 29] is developed to lay a basis for further discussion and to substantiate the efficacy of the proposed velocity-level RMP scheme (see Sect. 15.4).

The computer-aided design model of the mobile redundant robot manipulator is shown in Fig. 15.1, which is composed of a wheeled mobile platform and a six-DOF spatial robot manipulator. The mobile platform includes two independent drive wheels and two omnidirectional passive supporting wheels. In this chapter, only the end-effector position is considered, and thus the robot manipulator becomes a functionally redundant robot manipulator. As for such a mobile redundant robot manipulator, the integrated kinematics at the velocity level is obtained in the following form (with the detailed derivation being shown in [22]):

$$\dot{\mathbf{r}}_{\mathrm{w}} = J(\vartheta)\dot{\mathbf{q}}, \tag{15.1}$$

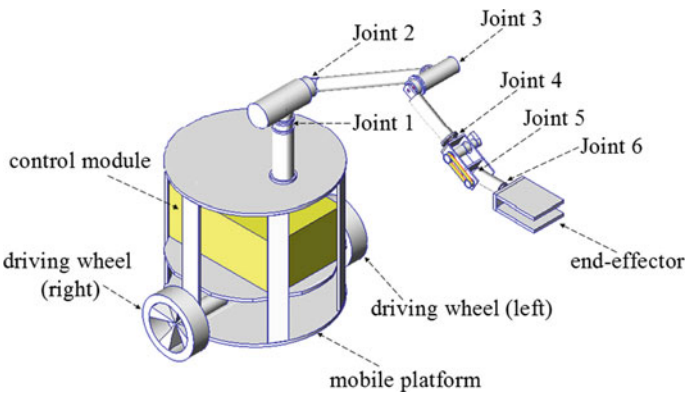

Fig. 15.1 The computer-aided design model of the mobile redundant robot manipulator

where $\dot{\mathbf{r}}_{\mathrm{w}} \in \mathbb{R}^m$ is the time derivative of the manipulator's end-effector position-and-orientation vector $\mathbf{r}_{\mathrm{w}}$ in Cartesian space with respect to the world coordinate frame. In addition, $J(\vartheta) \in \mathbb{R}^{m\times(2+n)}$ is the Jacobian matrix with vector $\vartheta = [\phi, \theta^{\mathrm{T}}]^{\mathrm{T}} \in \mathbb{R}^{1+n}$. Besides, $\phi \in \mathbb{R}$ is the heading angle of the mobile platform, and $\theta \in \mathbb{R}^n$ denotes the joint-angle vector of the six-DOF robot manipulator. Note that we define $\varphi = [\varphi_{\mathrm{l}}, \varphi_{\mathrm{r}}]^{\mathrm{T}} \in \mathbb{R}^2$ as the driving wheel angle (angular position) vector, with φ_{l} and φ_{r} being the angles of left and right driving wheel, respectively. Thus, we have the combined angle vector $\mathbf{q} = [\varphi^{\mathrm{T}}, \theta^{\mathrm{T}}]^{\mathrm{T}} \in \mathbb{R}^{2+n}$ for the presented mobile redundant robot manipulator, and its time derivative $\dot{\mathbf{q}} = [\dot{\varphi}^{\mathrm{T}}, \dot{\theta}^{\mathrm{T}}]^{\mathrm{T}}$ (i.e., the combined velocity vector).

15.2.2 Velocity-Level RMP Performance Index

In order to achieve the RMP purpose of the mobile robot manipulators, let us consider three factors of mobile robot manipulators, i.e., the joint angle of the robot manipulator $\theta \in \mathbb{R}^n$, the rotational angle of the mobile platform $\phi \in \mathbb{R}$ and the location of the robot manipulator on the mobile platform $\mathbf{p}_{\mathrm{C}} = [x_{\mathrm{C}}, y_{\mathrm{C}}]^{\mathrm{T}} \in \mathbb{R}^2$. Evidently, the mobile robot manipulator can return to the original state if and only if these three variables return to their initial positions, when the end-effector of mobile robot manipulators performs a closed trajectory. That is to say, the repetitive motion of mobile robot manipulators is equivalent to the repetitive motion of variables θ, ϕ, and $\mathbf{p}_{\mathrm{C}}$. Thus, by following the presented ZD approach, the repetitive motion of θ, ϕ, and $\mathbf{p}_{\mathrm{C}}$ can be achieved through the following design steps.

- First, to achieve the RMP purpose of the mobile robot manipulators, we define three different ZFs as follows:

$$\mathbf{e}(t) = \theta - \theta(0) \in \mathbb{R}^n, \tag{15.2}$$

$$e(t) = \sin\phi - \sin\phi(0) \in \mathbb{R}, \tag{15.3}$$

$$\mathbf{e}(t) = \mathbf{p}_{\mathrm{C}} - \mathbf{p}_{\mathrm{C}}(0) \in \mathbb{R}^2, \tag{15.4}$$

  where $\theta(0)$, $\phi(0)$, and $p_{\mathrm{C}}(0)$ denote the initial states of θ, ϕ and p_{C}, respectively. It is worth pointing out that, when the mobile platform moves circularly (i.e., the heading angle ϕ makes 360° turns), the heading angle can return to the initial position. In this situation, the value of the heading angle is $\phi = \phi(0) + 2k\pi$ ($k = \pm1, \pm2, \ldots$). If $\phi - \phi(0)$ is used [instead of $\sin\phi - \sin\phi(0)$], the restrictions become harsh and the resultant RMP scheme is difficult to realize. Thus, the sine function is exploited, and the simulation and modeling of the velocity-level RMP scheme become easy.
- Second, by combining the ZD design formula [27] and the above three ZFs, respectively [i.e., (4.2) corresponding to (15.2), (15.4), and (1.2) corresponding to (15.3)], three resultant differential equations are obtained as follows:

$$\dot{\theta} + \gamma_1(\theta - \theta(0)) = \mathbf{0} \in \mathbb{R}^n, \tag{15.5}$$

$$\dot{\phi}\cos\phi + \gamma_2(\sin\phi - \sin\phi(0)) = 0 \in \mathbb{R}, \tag{15.6}$$

$$\dot{\mathbf{p}}_{\mathrm{C}} + \gamma_3(\mathbf{p}_{\mathrm{C}} - \mathbf{p}_{\mathrm{C}}(0)) = \mathbf{0} \in \mathbb{R}^2. \tag{15.7}$$

For the above equations, $\dot{\theta} \in \mathbb{R}^n$ is the joint-velocity vector of the robot manipulator, $\dot{\phi} \in \mathbb{R}$ is the heading velocity of the mobile platform (being the time derivative of ϕ), and $\dot{\mathbf{p}}_{\mathrm{C}} \in \mathbb{R}^2$ is the time derivative of $\mathbf{p}_{\mathrm{C}}$. In addition, design parameters $\gamma_1 > 0 \in \mathbb{R}$, $\gamma_2 > 0 \in \mathbb{R}$, and $\gamma_3 > 0 \in \mathbb{R}$ are used for achieving the RMP purpose. In addition, one can prove theoretically that, in equations (15.5)–(15.7), as $t \to \infty$, θ, $\sin\phi$ and $\mathbf{p}_{\mathrm{C}}$ can converge to their initial states globally and exponentially.

- Third, in (15.1), the variables of the velocity-level integrated kinematics of the mobile root manipulator only include $\dot{\varphi}$ and $\dot{\theta}$ (i.e., $\dot{\mathbf{q}} = [\dot{\varphi}^{\mathrm{T}}, \dot{\theta}^{\mathrm{T}}]^{\mathrm{T}}$), so Eqs. (15.5)–(15.7) have to be converted into a $\dot{\mathbf{q}}$-based matrix-vector equation for meeting the needs of the simulation modeling. Note that, as for the mobile platform shown in Fig. 15.1, we have

$$A\dot{\varphi} = \dot{\phi} \quad \text{and} \quad B\dot{\varphi} = \dot{\mathbf{p}}_{\mathrm{C}},$$

where matrices A and B are defined respectively as follows:

$$A = \frac{r}{2b}\begin{bmatrix} -1 \\ 1 \end{bmatrix}^{\mathrm{T}} \in \mathbb{R}^{1\times 2}, \text{ and } B = \frac{r}{2}\begin{bmatrix} \cos\phi & -\sin\phi \\ \sin\phi & \cos\phi \end{bmatrix}\begin{bmatrix} 1 & 1 \\ -d/b & d/b \end{bmatrix} \in \mathbb{R}^{2\times 2},$$

with r being the radius of the drive wheels, b being the distance between the drive wheels and the middle point of the two-drive wheel axis (denoted as P_0), and d being the distance between the point connecting the robot manipulator and the mobile platform (corresponding to $\mathbf{p}_{\mathrm{C}}$) and point P_0. Thus, based on the above analysis, Eqs. (15.6) and (15.7) are merged into an equation in the form of

$$\begin{bmatrix} B \\ A\cos\phi \end{bmatrix}\dot{\varphi} + \begin{bmatrix} \gamma_3(\mathbf{p}_{\mathrm{C}} - \mathbf{p}_{\mathrm{C}}(0)) \\ \gamma_2(\sin\phi - \sin\phi(0)) \end{bmatrix} = \mathbf{0} \in \mathbb{R}^3. \tag{15.8}$$

- Fourth, by defining $\mathbf{a} = [\gamma_3(\mathbf{p}_{\mathrm{C}} - \mathbf{p}_{\mathrm{C}}(0)), \gamma_2(\sin\phi - \sin\phi(0))]^{\mathrm{T}} \in \mathbb{R}^3$, $C = [B^{\mathrm{T}}, A^{\mathrm{T}}\cos\phi]^{\mathrm{T}} \in \mathbb{R}^{3\times 2}$, and $\mathbf{c} = \gamma_1[\theta - \theta(0)] \in \mathbb{R}^n$, Eqs. (15.5) and (15.8) are further combined into a unified matrix-vector equation as follows:

$$D\dot{\mathbf{q}} + \mathbf{z} = \mathbf{0} \in \mathbb{R}^{n+3}, \tag{15.9}$$

where matrix D and vector z are defined respectively as

$$D = \begin{bmatrix} C & 0 \\ 0 & I \end{bmatrix} \in \mathbb{R}^{(n+3)\times(n+2)} \text{ and } \mathbf{z} = \begin{bmatrix} \mathbf{a} \\ \mathbf{c} \end{bmatrix} \in \mathbb{R}^{n+3},$$

with $I \in \mathbb{R}^{n\times n}$ being the identity matrix. Therefore, from the above derivation, one knows that solving (15.5)–(15.7) is equivalent to solving (15.9). In addition, when (15.9) is solved, the resultant solutions can achieve the RMP purpose of mobile redundant robot manipulators.

- Finally, because the end-effector motion-trajectory requirement has to be considered and physical constraints always exist in mobile manipulators, it is better to minimize $\|D\dot{\mathbf{q}}+\mathbf{z}\|_2^2/2$, rather than use $D\dot{\mathbf{q}}+\mathbf{z}=\mathbf{0}$ directly. Thus, we obtain

$$\|D\dot{\mathbf{q}}+\mathbf{z}\|_2^2/2 = (D\dot{\mathbf{q}}+\mathbf{z})^{\mathrm{T}}(D\dot{\mathbf{q}}+\mathbf{z})/2, \tag{15.10}$$

which is the velocity-level RMP performance index for mobile redundant robot manipulators.

In summary, by using the ZD approach, we have developed the RMP performance index (15.10) at the velocity level (showing the application prospect of such a ZD approach once again). Note that, by minimizing the velocity-level performance index (15.10) [i.e., "minimize $(D\dot{\mathbf{q}}+\mathbf{z})^{\mathrm{T}}(D\dot{\mathbf{q}}+\mathbf{z})/2$"], the RMP purpose is thus achieved for mobile redundant robot manipulators.

15.3 Scheme and QP Formulations

In this section, based on the proposed performance index (15.10), a novel velocity-level RMP scheme is further developed and investigated for mobile redundant robot manipulators. In addition, such an acceleration-level RMP scheme is reformulated as a QP, which is solved by a numerical algorithm.

15.3.1 Velocity-Level RMP Scheme

For mobile redundant robot manipulators, with physical limits considered, the velocity-level RMP scheme is proposed as follows:

$$\begin{aligned}
\text{minimize} \quad & (D\dot{\mathbf{q}}+\mathbf{z})^{\mathrm{T}}(D\dot{\mathbf{q}}+\mathbf{z})/2 && (15.11)\\
\text{subject to} \quad & J(\vartheta)\dot{\mathbf{q}} = \dot{\mathbf{r}}_{\mathrm{dw}}, && (15.12)\\
& \mathbf{q}^- \leqslant \mathbf{q} \leqslant \mathbf{q}^+, && (15.13)\\
& \dot{\mathbf{q}}^- \leqslant \dot{\mathbf{q}} \leqslant \dot{\mathbf{q}}^+, && (15.14)
\end{aligned}$$

where $\dot{\mathbf{r}}_{\mathrm{dw}} \in \mathbb{R}^m$ denotes the time derivative of the desired end-effector path $\mathbf{r}_{\mathrm{dw}}$. In addition, $\mathbf{q}^-$ and $\mathbf{q}^+$ denote respectively the lower and upper limits of the combined angle vector $\mathbf{q}$. Furthermore, $\dot{\mathbf{q}}^-$ and $\dot{\mathbf{q}}^+$ denote respectively the lower and upper limits of the combined velocity vector $\dot{\mathbf{q}}$. Note that the physical limits (i.e., $\mathbf{q}^-$, $\mathbf{q}^+$,

Table 15.1 The physical limits used in the wheeled mobile robot manipulator shown in Fig. 15.1

i	1	2	3	4	5	6	7	8
q_i^- (rad)	$-\infty$	$-\infty$	-0.5236	-0.1745	-6.2832	-6.2832	-6.2832	-6.2832
q_i^+ (rad)	$+\infty$	$+\infty$	$+0.5236$	$+2.3562$	$+6.2832$	$+6.2832$	$+6.2832$	$+6.2832$
$\dot{q}_i^-$ (rad/s)	-30.0000	-30.0000	-3.0000	-3.0000	-3.0000	-3.0000	-3.0000	-3.0000
$\dot{q}_i^+$ (rad/s)	$+30.0000$	$+30.0000$	$+3.0000$	$+3.0000$	$+3.0000$	$+3.0000$	$+3.0000$	$+3.0000$

$\dot{\mathbf{q}}^-$ and $\dot{\mathbf{q}}^+$) used in the wheeled mobile robot manipulator shown in Fig. 15.1 are presented in Table 15.1.

15.3.2 QP Reformulation

As the proposed RMP scheme (15.11)–(15.14) is resolved at the combined-vector velocity level (i.e., in terms of $\dot{\mathbf{q}}$), the limited combined angle vector range $[\mathbf{q}^-, \mathbf{q}^+]$ has to be converted into a $\dot{\mathbf{q}}$-based expression. The following conversion technique is adopted:

$$\mu(\mathbf{q}^- - \mathbf{q}) \leqslant \dot{\mathbf{q}} \leqslant \mu(\mathbf{q}^+ - \mathbf{q}),$$

where $\mu > 0 \in \mathbb{R}$ is used to scale the feasible region of $\dot{q}$. Note that large values of μ may cause sudden deceleration for joints and wheels when the mobile robot manipulator approaches their physical limits, and that, in mathematically, $\mu \geqslant 2\max_{1\leqslant i\leqslant n+2}\{\dot{q}_i^+/(q_i^+ - q_i^-), -\dot{q}_i^-/(q_i^+ - q_i^-)\}$. Therefore, the following new combined bound constraints can be used to replace (15.13) and (15.14):

$$\zeta^- \leqslant \dot{\mathbf{q}} \leqslant \zeta^+,$$

where the ith elements of ζ^- and ζ^+ are, respectively, defined as (with $i = 1, 2, \ldots, n+2$) $\zeta_i^- = \max\{\mu(q_i^- - q_i), \dot{q}_i^-\}$ and $\zeta_i^+ = \min\{\mu(q_i^+ - q_i), \dot{q}_i^+\}$.

By summarizing the above analysis and defining the decision variable vector $\mathbf{x} = \dot{\mathbf{q}} \in \mathbb{R}^{n+2}$, the proposed RMP scheme (15.11)–(15.14) for mobile redundant robot manipulators is reformulated as the following QP, in view of $(D\mathbf{x}+\mathbf{z})^{\mathrm{T}}(D\mathbf{x}+\mathbf{z})/2 = \mathbf{x}^{\mathrm{T}}D^{\mathrm{T}}D\mathbf{x}/2 + \mathbf{z}^{\mathrm{T}}D\mathbf{x} + \mathbf{z}^{\mathrm{T}}\mathbf{z}/2$:

$$\begin{aligned} \text{minimize} \quad & \mathbf{x}^{\mathrm{T}}W\mathbf{x}/2 + \mathbf{h}^{\mathrm{T}}\mathbf{x} && (15.15)\\ \text{subject to} \quad & C\mathbf{x} = \mathbf{d}, && (15.16)\\ & \zeta^- \leqslant \mathbf{x} \leqslant \zeta^+, && (15.17) \end{aligned}$$

where $W = D^{\mathrm{T}}D \in \mathbb{R}^{(n+2)\times(n+2)}$, $C = J(\vartheta) \in \mathbb{R}^{m\times(n+2)}$, $\mathbf{h} = D^{\mathrm{T}}\mathbf{z} \in \mathbb{R}^{n+2}$, and $d = \dot{\mathbf{r}}_{\mathrm{dw}} \in \mathbb{R}^m$. As for the above QP, the performance criterion (15.15) is for the RMP purpose and results from the simplification of (15.11). The equality constraint (15.16) [i.e., (15.1) or (15.12)] describes the integrated kinematics relationship of mobile robot manipulators at the combined-vector velocity level. The inequality constraint (15.17) is used to equivalently replace constraints (15.13) and (15.14) by exploiting a conversion technique.

15.3.3 QP Solver

Note that the presented QP formulation [i.e., (15.15)–(15.17)] is the same as the one shown in Chap. 14. Thus, the PDNN (14.18) can also be used to solve such a QP problem (15.15)–(15.17). In this subsection, being different from the PDNN, a numerical algorithm is exploited to solve the presented QP problem [as well as the proposed RMP scheme (15.11)–(15.14)].

In order to solve the QP problem (15.15)–(15.17), guided by [5, 6, 22, 30–32], we define the following vector-valued error function:

$$\mathbf{e}(\mathbf{u}) = \mathbf{u} - P_{\Omega}(\mathbf{u} - (M\mathbf{u} + \mathbf{p})) \in \mathbb{R}^{n+m+2}, \tag{15.18}$$

where the formulations of matrix $M \in \mathbb{R}^{(n+m+2)\times(n+m+2)}$, vectors $\mathbf{u} \in \mathbb{R}^{n+m+2}$ and $\mathbf{p} \in \mathbb{R}^{n+m+2}$ are presented the same as those shown in Chap. 14, and $P_{\Omega}(\cdot)$ is the projection operator.

Let $\mathbb{S} = \{\mathbf{u}^* | \mathbf{u}^* \text{is a zero point of (15.18)}\}$. When the initial value of primal–dual decision variable vector $\mathbf{u}^0 \in \mathbb{R}^{n+m+2}$ is given, for iteration index $k = 0, 1, 2, \ldots$, if $\mathbf{u}^k \notin \mathbb{S}$, we have the following iteration formula for finding a zero point of (15.18) [as well as for solving QP (15.15)–(15.17)]:

$$\mathbf{u}^{k+1} = \mathbf{u}^k - \frac{\|\mathbf{e}(\mathbf{u}^k)\|_2^2}{\|(M^{\mathrm{T}} + I)\mathbf{e}(\mathbf{u}^k)\|_2^2}(M^{\mathrm{T}} + I)\mathbf{e}(\mathbf{u}^k), \tag{15.19}$$

where $I \in \mathbb{R}^{(n+m+2)\times(n+m+2)}$ is the identity matrix.

An important criterion of measuring the performance of numerical algorithms is their computational complexity. As seen from the above iteration formula (15.19), within one iteration, it only contains $2\hat{\alpha}^2 + 3\alpha + 1$ multiplications and $2\hat{\alpha}^2 + 5\hat{\alpha} - 2$ additions, with $\hat{\alpha} = n + m + 2$. Therefore, the discrete-time QP solver (15.19) has a low computational complexity; i.e., $O(\hat{\alpha}^2)$. In addition, we usually choose the solution obtained in the previous time step as the initial value of the new time step, as such, the discrete-time QP solver (15.19) has better real-time performance. Besides, by following [5, 22, 30, 31], an important theorem about the global convergence of the discrete-time QP solver (15.19) is presented.

Theorem 15.1 *The sequence* $\{\mathbf{u}^k\}$ *generated by the discrete-time solver (15.19) for (15.18) as well as for QP (15.15)–(15.17) satisfies*

$$\|\mathbf{u}^{k+1} - \mathbf{u}^*\|_2^2 \leqslant \|\mathbf{u}^k - \mathbf{u}^*\|_2^2 - \|\mathbf{e}(\mathbf{u}^k)\|_2^2 / \|M^{\mathrm{T}} + I\|_{\mathrm{F}}^2$$

for all $u^* \in \mathbb{S}$. *In addition, the sequence* $\{\mathbf{u}^k\}$ *globally converges to a solution* $\mathbf{u}^*$, *of which the first* $(n + 2)$ *elements constitute the optimal solution* $\mathbf{x}^*$ *to QP (15.15)–(15.17).*

15.4 Illustrative Examples

In this section, computer simulations are conducted on the wheeled mobile redundant robot manipulator shown in Fig. 15.1 to substantiate the efficacy of the proposed RMP scheme (15.11)–(15.14). Note that the final error tolerance of $\|\mathbf{e}(\mathbf{u}^k)\|_2$ is set to be 1.0×10^{-6} for discrete-time QP solver (15.19). In the first example, the end-effector of the mobile robot manipulator is expected to track a circular path, and in the second example the end-effector is to follow a Lissajous path. Without loss of generality, we set $\mu = 2$, initial state $\theta(0) = [\pi/12, \pi/3, \pi/3, \pi/3, \pi/3, \pi/3]^{\mathrm{T}}$ rad, and $\phi(0) = x_{\mathrm{C}}(0) = y_{\mathrm{C}}(0) = 0$ rad, for the wheeled mobile robot manipulator.

15.4.1 Circular Path Tracking

In this subsection, the end-effector of the wheeled mobile robot manipulator is expected to track a circular path with radius ψ being 0.3 m. The X-axis, Y-axis, and Z-axis functions of the desired circular path are

$$\begin{cases} \dot{r}_{\mathrm{dwX}}(t) = -\frac{2\pi^2\psi}{T}\sin(2\pi\,\sin^2(\frac{\pi t}{2T}) + \pi/6)\sin(\frac{\pi t}{2T})\cos(\frac{\pi t}{2T}), \\ \dot{r}_{\mathrm{dwY}}(t) = \frac{2\pi^2\psi}{T}\cos(2\pi\,\sin^2(\frac{\pi t}{2T}) + \pi/6)\sin(\frac{\pi t}{2T})\cos(\frac{\pi t}{2T}), \\ \dot{r}_{\mathrm{dwZ}}(t) = 0, \end{cases}$$

where task duration $T = 5$ s and $t \in [0, T]$.

Non-repetitive motion First, we show the non-repetitive motion of the mobile robot manipulator. Since γ_1, γ_2 and γ_3 are greater than zero, a non-repetitive motion scheme is produced when $\gamma_1 = \gamma_2 = \gamma_3 = 0$. In this situation, the circular-path tracking results are shown in Fig. 15.2. The upper graph of Fig. 15.2 shows the whole tracking process of the mobile robot manipulator. It follows from such a graph that the final state of the mobile robot manipulator does not return to the initial one, i.e., the solution in this situation is not repetitive. For a better understanding, the middle graph of Fig. 15.2 shows the top view of motion trajectories of the mobile robot manipulator, and the lower graph of Fig. 15.2 shows the motion trajectories of the mobile platform. It follows from such two graphs that the mobile platform is not repetitive after the end-effector completing the circular-path tracking task. Besides, Fig. 15.3 shows profiles of point of junction $[x_{\mathrm{C}}, y_{\mathrm{C}}]^{\mathrm{T}}$, heading angle ϕ, joint angle θ, left and right wheels synthesized by the non-repetitive motion scheme when the mobile robot manipulator tracks the given circular path. From Fig. 15.3, we can see that these variables do not return to their initial values. In engineering applications, this situation may induce a problem wherein the behavior of the mobile robot manipulator is hard to predict. Readjusting the configuration of the manipulator through self-motion is inefficient.

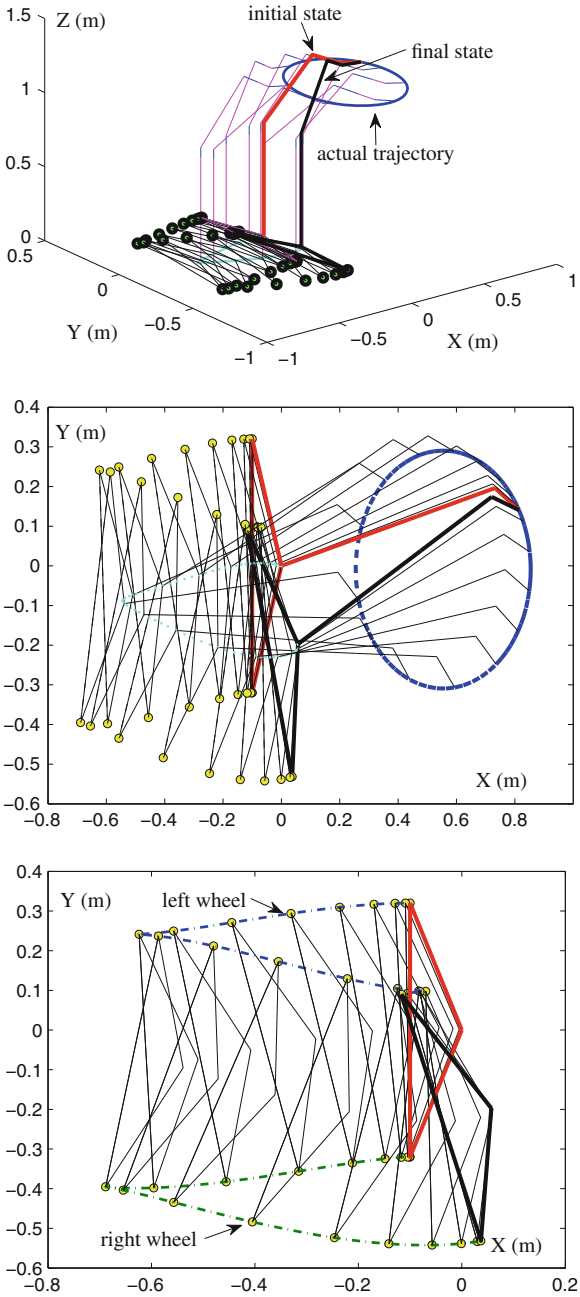

Fig. 15.2 Simulation results when the mobile robot manipulator tracks the given circular path synthesized by the non-repetitive motion scheme

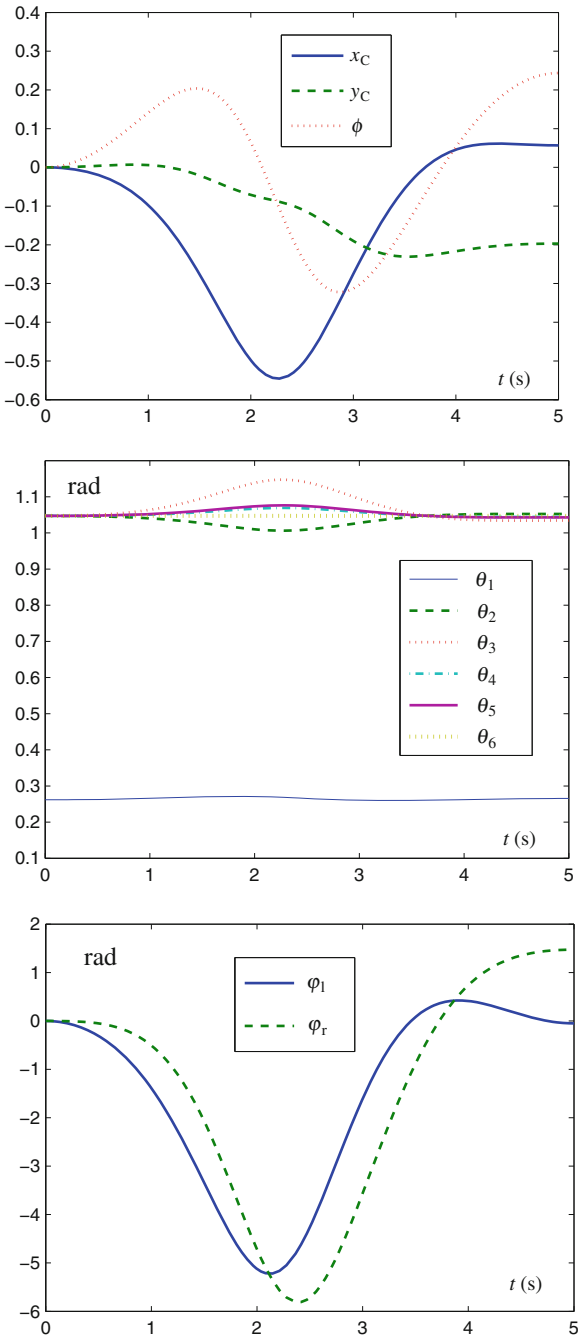

Fig. 15.3 Profiles of point of junction $[x_C, y_C]^T$, heading angle ϕ, joint angle θ, *left* and *right* wheels for the mobile robot manipulator synthesized by the non-repetitive motion scheme

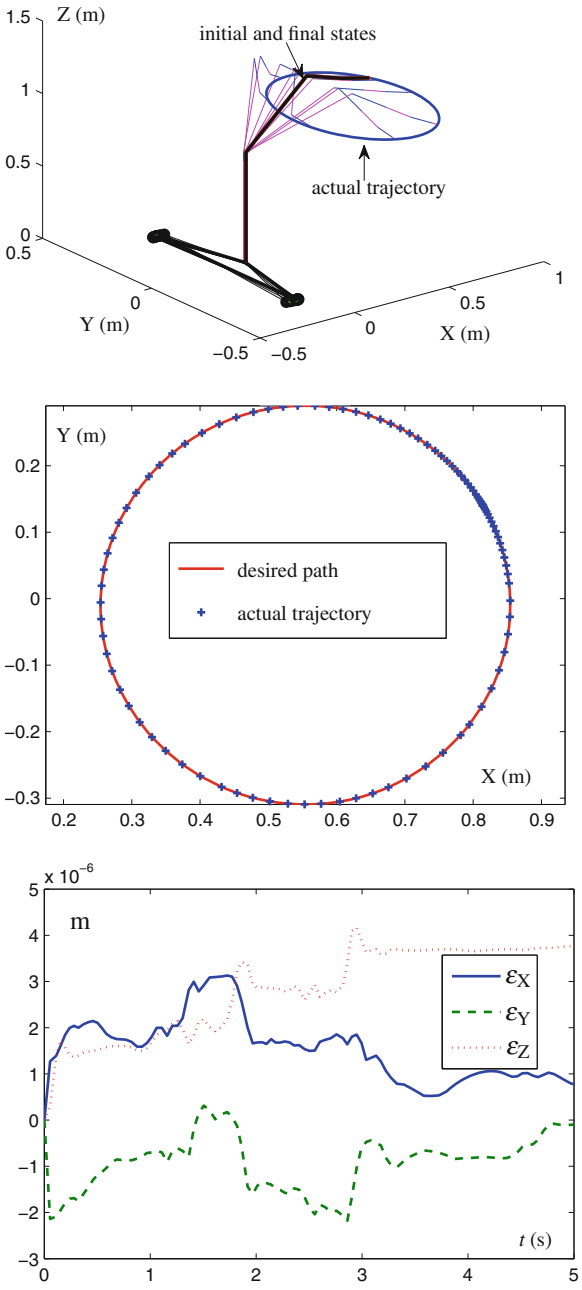

Fig. 15.4 Simulation results when the mobile robot manipulator tracks the given circular path synthesized by the proposed RMP scheme (15.11)–(15.14)

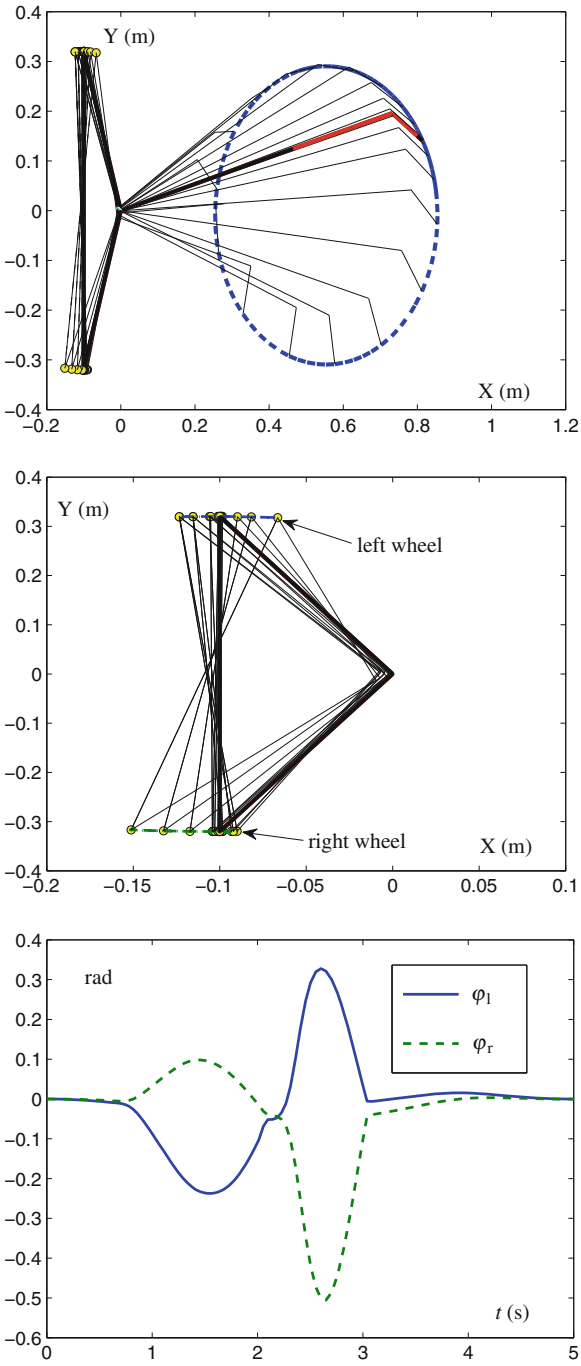

Fig. 15.5 More simulation results when the mobile robot manipulator tracks the given circular path synthesized by the proposed RMP scheme (15.11)–(15.14)

Repetitive motion To finish the circular-path tracking task in a repetitive manner, the proposed RMP scheme (15.11)–(15.14) with $\gamma_1 = \gamma_2 = \gamma_3 = 10^5$ and the discrete-time QP solver are applied to the control of the mobile robot manipulator. The corresponding simulation results are shown in Figs. 15.4, 15.5, 15.6, and 15.7.

Specifically, the upper graph of Fig. 15.4 shows the motion trajectories of the mobile robot manipulator during the whole tracking process. As seen from such a graph, the proposed RMP scheme (15.11)–(15.14) not only coordinates simultaneously the mobile platform and the manipulator to complete the given end-effector task, but also makes the mobile manipulator return to the initial state. In addition, from the middle graph of Fig. 15.4, we can see that the actual end-effector motion trajectory is close enough to the desired circular path. The lower graph of Fig. 15.4 shows the corresponding tracking position errors. As seen from such a graph, the corresponding X-axis, Y-axis, and Z-axis components of the tracking position error are less than 5×10^{-6} m. These results substantiate that the mobile robot manipulator

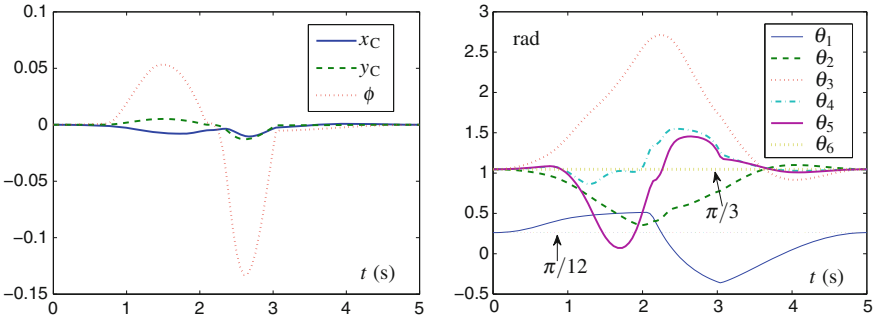

Fig. 15.6 Profiles of point of junction $[x_C, y_C]^T$, heading angle ϕ and joint angle θ when the mobile robot manipulator tracks the given circular path synthesized by the proposed RMP scheme (15.11)–(15.14)

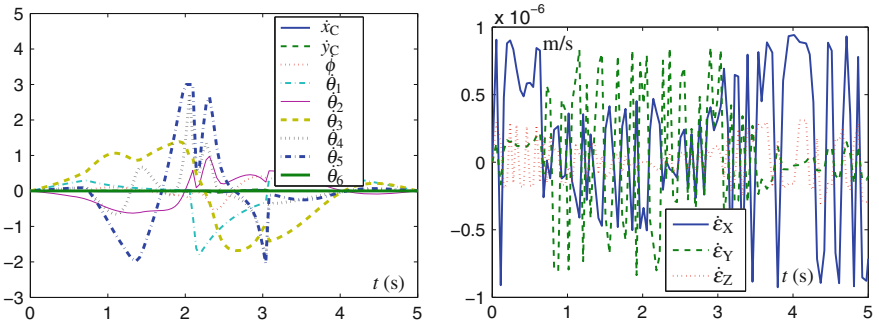

Fig. 15.7 Profiles of $[\dot{x}_C, \dot{y}_C]^T$, heading velocity $\dot{\phi}$, joint velocity $\dot{\theta}$ and the corresponding tracking velocity error when the mobile robot manipulator tracks the given circular path synthesized by the proposed RMP scheme (15.11)–(15.14)

can finish the circular path tracking task well, as synthesized by the proposed RMP scheme (15.11)–(15.14).

To further illustrate and verify the effectiveness of the proposed RMP scheme (15.11)–(15.14), in Fig. 15.5, we show the movements of the mobile platform. Specifically, the upper graph of Fig. 15.5 shows the top view of motion trajectories of the mobile robot manipulator, the middle graph of Fig. 15.5 shows the motion trajectories of the mobile platform, and the lower graph of Fig. 15.5 shows the corresponding left and right wheel profiles. From Fig. 15.5, we can conclude that the mobile platform is repetitive after the end-effector completing the circular-path tracking task.

Besides, what we are more interested in are some important variables, such as point of junction $[x_C, y_C]^T$, heading angle ϕ and joint angle θ. This reason lies in that if and only if these variables return to their initial states, the mobile manipulator can achieve the repetitive motion. Figure 15.6 shows the profiles of $[x_C, y_C]^T$, ϕ, and θ when the mobile manipulator tracks the given circular path. As seen from the left graph of Fig. 15.6, x_C, y_C, and ϕ return to their initial states. In addition, the right graph of Fig. 15.6 shows that θ also returns to its initial state $\theta(0)$. That is to say, these variables all return to their initial states, so that the mobile robot manipulator can achieve the repetitive motion. Figure 15.7 shows the profiles of $[\dot{x}_C, \dot{y}_C]^T$, heading velocity $\dot{\phi}$, joint velocity $\dot{\theta}$, and the corresponding tracking velocity error when the mobile manipulator tracks the given circular path. From Fig. 15.7, we can see that the final states of the combined velocity equal zero, and that the corresponding X-axis, Y-axis, and Z-axis components of the tracking velocity error are less 1×10^{-6} m. The results further substantiate the high accuracy of the proposed RMP scheme (15.11)–(15.14). It is worth pointing out that, in the left graph of Fig. 15.7, $\dot{\theta}_5$ reaches its upper bound $\dot{\theta}_5^+$, but never exceed the upper bound, which demonstrates that the bound constraint (15.14) is activated and effective.

15.4.2 Lissajous-Figure Path Tracking

In this subsection, the end-effector of the mobile robot manipulator is expected to track a Lissajous-figure path with parameter χ being 0.45 m. The X-axis, Y-axis, and Z-axis velocity functions of the desired Lissajous-figure path are

$$\begin{cases} \dot{r}_{dwX}(t) = -\frac{4\pi^2\chi}{T} \sin(4\pi \sin^2(\frac{\pi t}{2T}) + \pi/6) \sin(\frac{\pi t}{2T}) \cos(\frac{\pi t}{2T}), \\ \dot{r}_{dwY}(t) = \frac{2\pi^2\chi}{T} \cos(2\pi \sin^2(\frac{\pi t}{2T}) + \pi/6) \sin(\frac{\pi t}{2T}) \cos(\frac{\pi t}{2T}), \\ \dot{r}_{dwZ}(t) = 0. \end{cases}$$

In order to investigate the effectiveness of the proposed RMP scheme (15.11)–(15.14) for different values of parameters, in this example, we set task duration $T = 10$ s, $\gamma_1 = \gamma_2 = 10^3$, and $\gamma_3 = 10^2$. Thus, the corresponding simulation results, synthesized by the proposed RMP scheme (15.11)–(15.14) and the discrete-time QP solver (15.19), are shown in Figs. 15.8, 15.9, 15.10, and 15.11.

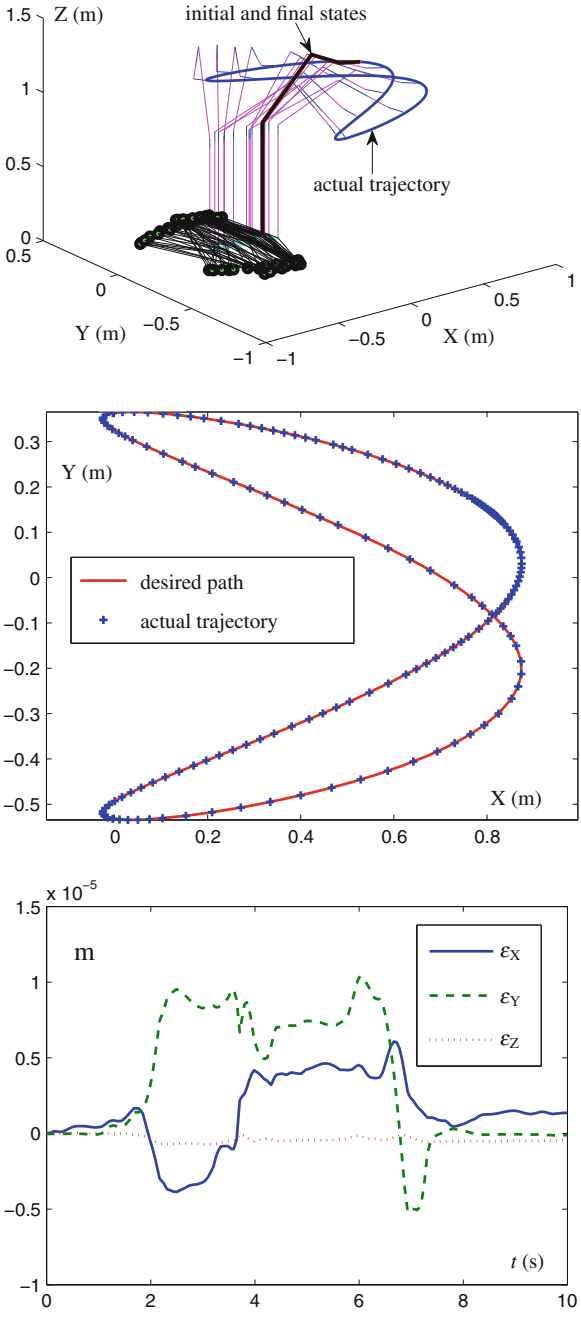

Fig. 15.8 Simulation results when the mobile robot manipulator tracks the given Lissajous-figure path synthesized by the proposed RMP scheme (15.11)–(15.14)

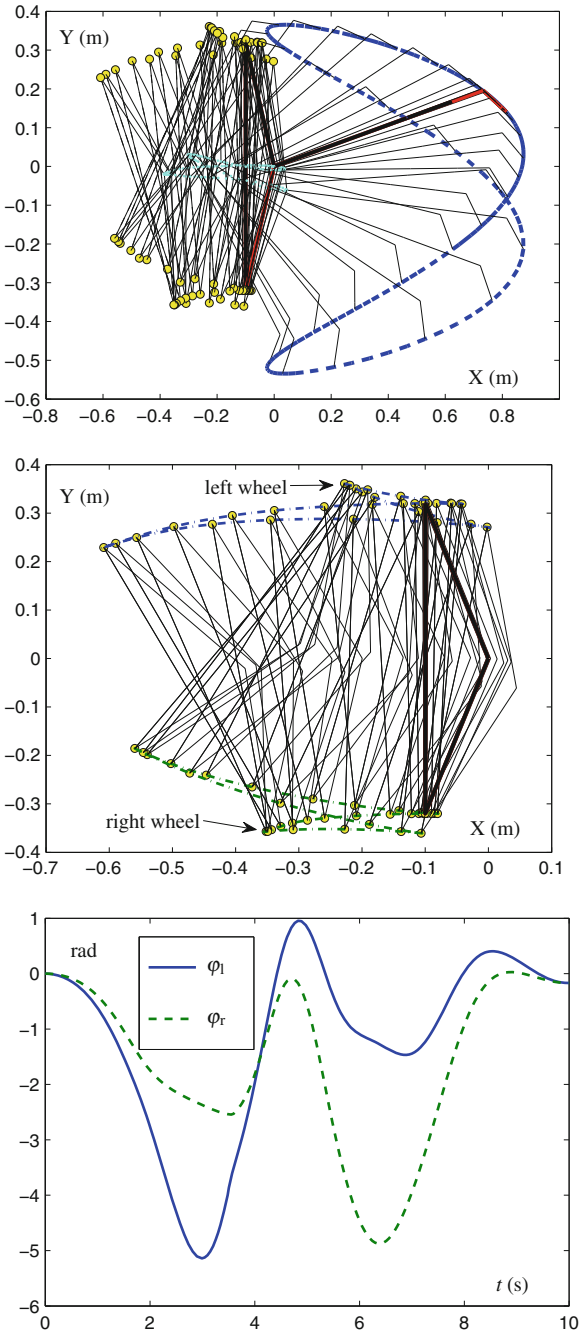

Fig. 15.9 More simulation results when the mobile robot manipulator tracks the given Lissajous-figure path synthesized by the proposed RMP scheme (15.11)–(15.14)

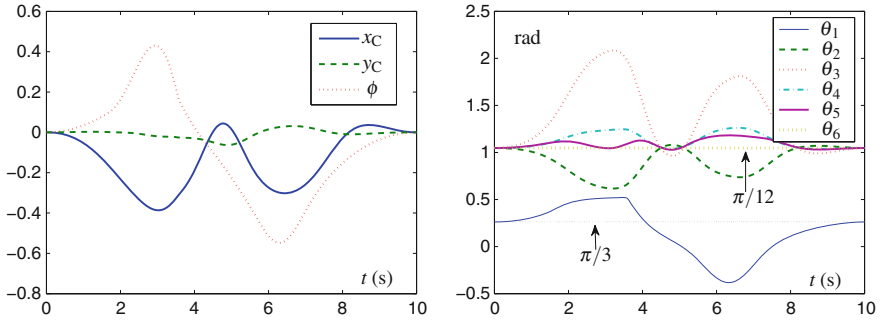

Fig. 15.10 Profiles of point of junction $[x_C, y_C]^T$, heading angle ϕ and joint angle θ when the mobile robot manipulator tracks the given Lissajous-figure path synthesized by the proposed RMP scheme (15.11)–(15.14)

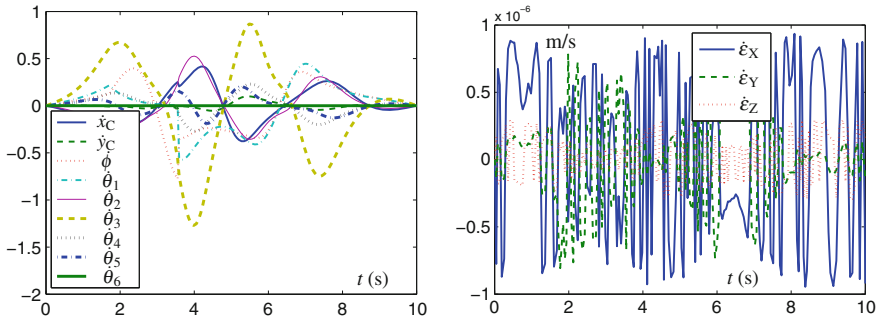

Fig. 15.11 Profiles of $[\dot{x}_C, \dot{y}_C]^T$, heading velocity $\dot{\phi}$, joint velocity $\dot{\theta}$, and the corresponding tracking velocity error when the mobile robot manipulator tracks the given Lissajous-figure path synthesized by the proposed RMP scheme (15.11)–(15.14)

The upper graph of Fig. 15.8 shows the whole tracking process of the mobile robot manipulator. As seen from such a graph, the RMP purpose of the mobile robot manipulator is achieved. Besides, the middle graph of Fig. 15.8 shows the desired Lissajous-figure path and the actual end-effector trajectory, and the lower graph of Fig. 15.8 shows the corresponding tracking position errors. As observed from the middle graph of Fig. 15.8, the actual motion trajectory of the mobile robot manipulator's end-effector is sufficiently close to the desired Lissajous-figure path. The corresponding X-axis, Y-axis, and Z-axis components of the tracking position error shown in the lower graph of Fig. 15.8 are less than 1×10^{-5} m. These demonstrate that the given Lissajous-figure path tracking task is performed well via the proposed RMP scheme (15.11)–(15.14).

To see more clearly the repetitive motion of the mobile robot manipulator, its mobile platform is visualized in Fig. 15.9. Specifically, the upper graph of Fig. 15.9 shows the top view of motion trajectories of the mobile robot manipulator, the middle graph of Fig. 15.9 shows the motion trajectories of the mobile platform, and the lower

graph of Fig. 15.9 shows the corresponding left and right wheel profiles. It follows from Fig. 15.9 that the mobile platform is repetitive after the end-effector completing the Lissajous-figure path tracking task.

Figure 15.10 shows the profiles of $[x_C, y_C]^T$, ϕ, and θ when the mobile manipulator tracks the given Lissajous path. As seen from the left graph of Fig. 15.10, x_C, y_C, and ϕ go back to their initial states. In addition, the right graph of Fig. 15.10 shows that θ also returns to its initial state $\theta(0)$. These illustrate and verify again the effectiveness of such a repetitive motion scheme and the non-repetitive problem of the mobile manipulator has been solved by using the repetitive motion scheme. Figure 15.11 further shows the profiles of $[\dot{x}_C, \dot{y}_C]^T$, heading velocity $\dot{\phi}$, joint velocity $\dot{\theta}$ and the corresponding tracking velocity error when the mobile manipulator tracks the given Lissajous path. From the left graph of Fig. 15.11, we can see that the final states of the combined velocity equal zero. Note that, if the final states of combined velocity are not zero, the mobile manipulator will not stop immediately at the end of the task duration; and thus the non-repetitive problem may happen. From the right graph of Fig. 15.11, one can see that the corresponding X-axis, Y-axis, and Z-axis components of the tracking velocity error are less 1×10^{-6} m. The results further demonstrate the high accuracy of the proposed RMP scheme (15.11)–(15.14) and discrete-time QP solver (15.19). It is also worth noting that all the variables (e.g., θ, $\dot{\theta}$, ϕ, and φ) in simulations are kept within their limits due to consideration of physical constraints of mobile manipulators. Thus, the given end-effector task can be completed successfully.

In summary, the presented two examples performed on the wheeled mobile robot manipulator, i.e., tracking a circular path and a Lissajous-figure path, have both substantiated the efficacy of the proposed RMP scheme (15.11)–(15.14) and the corresponding discrete-time QP solver (15.19), which can solve the non-repetitive problem well. Furthermore, the tracking position and velocity errors shown in Figs. 15.4, 15.7, 15.8 and 15.11, have validated well the high accuracy of such a RMP scheme (15.11)–(15.14). Besides, these simulation results have shown again the successful application of the presented ZD approach to RMP of mobile redundant robot manipulators.

15.5 Summary

In this chapter, by defining three different ZFs and by exploiting the ZD design formula, the velocity-level RMP performance index (15.10) has been proposed, developed, and investigated. Based on such a performance index, the velocity-level RMP scheme (15.11)–(15.14) has been further presented and investigated for mobile redundant robot manipulators, which is reformulated as a QP (15.15)–(15.17) and then is solved by the numerical algorithm (15.19). Computer simulation results based on the wheeled mobile robot manipulator with different illustrative examples have substantiated well the effectiveness, accuracy, and safety of the proposed velocity-level

RMP scheme for physically-constrained mobile redundant robot manipulators, and more importantly, have shown once again the application prospect of the presented ZD approach to robotic redundancy resolution.

References

1. Lasky TA, Ravani B (2000) Sensor-based path planning and motion control for a robotic system for roadway crack sealing. IEEE Trans Control Syst Technol 8(4):609–622
2. Xia Y, Wang J (2001) A dual neural network for kinematic control of redundant robot manipulators. IEEE Trans Syst, Man, Cybern B 31(1):147–154
3. Shahri NR, Troch I (1996) Collision-avoidance for redundant robots through control of the self-motion of the manipulator. J Intell Robot Syst 16(2):123–149
4. Ding H, Chan SP (1996) A real-time planning algorithm for obstacle avoidance of redundant robots. J Intell Robot Syst 16(3):229–243
5. Zhang Y, Zhang Z (2013) Repetitive motion planning and control of redundant robot manipulators. Springer, New York
6. Guo D, Zhang Y (2014) Acceleration-level inequality-based MAN scheme for obstacle avoidance of redundant robot manipulators. IEEE Trans Ind Electron 61(12):6903–6914
7. Guo D, Zhang Y (2014) Simulation and experimental verification of weighted velocity and acceleration minimization for robotic redundancy resolution. IEEE Trans Autom Sci Eng 11(4):1203–1217
8. Guo D, Zhang Y (2014) Li-function activated ZNN with finite-time convergence applied to redundant-manipulator kinematic control via time-varying Jacobian matrix pseudoinversion. Appl Soft Comput 24:158–168
9. Klein CA, Kee KB (1989) The nature of drift in pseudoinverse control of kinematically redundant manipulators. IEEE Trans Robot Autom 5(2):231–234
10. Klein CA, Ahmed S (1995) Repeatable pseudoinverse control for planar kinematically redundant manipulators. IEEE Trans Syst, Man, Cybern 25(12):1657–1662
11. Siciliano B, Khatib O (2008) Springer handbook of robotics. Springer, Heidelberg
12. Siciliano B, Sciavicco L, Villani L, Oriolo G (2009) Robotics: modelling, planning and control. Springer, London
13. Zhang Z, Zhang Y (2012) Acceleration-level cyclic-motion generation of constrained redundant robots tracking different paths. IEEE Trans Syst Man Cybern B 42(4):1257–1269
14. Zhang Y, Tan Z, Chen K, Yang Z, Lv X (2009) Repetitive motion of redundant robots planned by three kinds of recurrent neural networks and illustrated with a four-link planar manipulator's straight-line example. Robot Auton Syst 57(6–7):645–651
15. Zhang Y, Lv X, Li Z, Yang Z, Chen K (2008) Repetitive motion planning of PA10 robot arm subject to joint physical limits and using LVI-based primal-dual neural network. Mechatronics 18(9):475–485
16. Shamir T, Yomdin Y (1988) Repeatability of redundant manipulators: Mathematical solution of the problem. IEEE Trans Autom Control 33(6):1004–1009
17. Roberts RG, Maciejewski AA (1993) Repeatable generalized inverse control strategies for kinematically redundant manipulators. IEEE Trans Autom Control 38(5):689–698
18. Tchon K, Jakubiak J (2005) A repeatable inverse kinematics algorithm with linear invariant subspaces for mobile manipulators. IEEE Trans Syst, Man, Cybern B 35(5):1051–1057
19. Lee JK, Cho HS (1997) Mobile manipulator motion planning for multiple tasks using global optimization approach. J Intell Robot Syst 18(2):169–190
20. Bayle B, Fourquet J-Y,M. Renaud M (2003) Manipulability of wheeled mobile manipulators: Application to motion generation. Int J Robot Res 22(7–8):565–581

21. Xu D, Zhao D, Yi J, Tan X (2009) Trajectory tracking control of omnidirectional wheeled mobile manipulators: Robust neural networkbased sliding mode approach. IEEE Trans Syst, Man, Cybern B 39(3):788–799
22. Xiao L, Zhang Y (2014) A new performance index for the repetitive motion of mobile manipulators. IEEE Trans Cybern 44(2):280–292
23. Tchoń K (2002) Repeatability of inverse kinematics algorithms for mobile manipulators. IEEE Trans Autom Control 47(8):1376–1380
24. Tchoń K, Jakubiak J (2003) Endogenous configuration space approach to mobile manipulators: a derivation and performance assessment of Jacobian inverse kinematics algorithms. Int J Control 76:1387–1419
25. Tchoń K, Jakubiak J (2005) A repeatable inverse kinematics algorithm with linear invariant subspaces for mobile manipulators. IEEE Trans Syst, Man, Cybern B 35(5):1051–1057
26. Tchoń K (2006) Repeatable, extended Jacobian inverse kinematics algorithm for mobile manipulators. Syst Control Lett 55:87–93
27. Zhang Y, Yi C (2011) Zhang neural networks and neural-dynamic method. Nova Science Publishers, New York
28. Tang C, Miller P, Krovi V, Ryu J, Agrawal S (2011) Differential-flatness-based planning and control of a wheeled mobile manipulator-Theory and experiment. IEEE/ASME Trans Mechatron 16(4):768–773
29. White GD, Bhatt RM, Tang CP, Krovi VN (2009) Experimental evaluation of dynamic redundancy resolution in a nonholonomic wheeled mobile manipulator. IEEE/ASME Trans Mechatron 14(3):349–357
30. He B (1994) Solving a class of linear projection equations. Numer Math 68(1):71–80
31. He B (1994) A new method for a class of linear variational inequalities. Math Program 66(2):137–144
32. Guo D, Zhang Y (2012) A new inequality-based obstacle-avoidance MVN scheme and its application to redundant robot manipulators. IEEE Trans Syst, Man, Cybern, C 42(6):1326–1340